RSC Advances

PAPER

View Article Online
View Journal | View Issue

Cite this: *RSC Adv.*, 2022, **12**, 25962

Supercritical CO_2 assisted extraction of essential oil and naringin from *Citrus grandis* peel: *in vitro* antimicrobial activity and docking study†

Thanh-Chi Mai,*[ab] Ngoc-Thinh Tran,[a] Dinh-Tri Mai,[ab] Tran Thi Ngoc Mai,[c] Nguyen Hong Thuc Duyen,[d] Tran Nguyen Minh An,*[d] Mahboob Alam,[e] Chi-Hien Dang[ab] and Thanh-Danh Nguyen *[ab]

The extraction of bioactive compounds, including essential oils and flavonoids, using organic solvents is a significant environmental concern. In this work, waste *C. grandis* peel was the ingredient used to extract essential oil and naringin by conducting a supercritical CO_2 technique with a two stage process. In the first stage, the extraction with only supercritical CO_2 solvent showed a significant enhancement of the D-limonene component, up to 95.66% compared with the hydro-distillation extraction (87.60%). The extraction of naringin using supercritical CO_2 and ethanol as a co-solvent was done in the second stage of the process, followed by evaluating *in vitro* antimicrobial activity of both the essential oil and naringin. The essential oil indicated significant activity against *M. catarrhalis* (0.25 mg ml^{-1}), *S. pyogenes* (1.0 mg ml^{-1}), *S. pneumoniae* (1.0 mg ml^{-1}). Whilst naringin gave good inhibition towards all tested microbial strains with MIC values in the range of 6.25–25.0 μM. In particular, naringin exhibited high antifungal activity against *T. rubrum*, *T. mentagrophytes*, and *M. gypseum*. The molecular docking study also confirmed that D-limonene inhibited bacterium *M. catarrhalis* well and that naringin possessed potential ligand interactions that proved the inhibition effective against fungi. Molecular dynamics simulations of naringin demonstrated the best docking model using Gromacs during simulation up to 100 ns to explore the stability of the complex naringin and crystal structure of enzyme 2VF5: PDB.

Received 1st July 2022
Accepted 1st September 2022

DOI: 10.1039/d2ra04068a

rsc.li/rsc-advances

1. Introduction

The *Citrus grandis* species that is distributed worldwide is the largest citrus fruit from the family Rutaceae and is consumed mostly in Southeast Asia. *C. grandis* fruits are not only served as food but are also considered as a traditional medicine around the world.[1] Although the peel of *C. grandis* fruits mainly contains flavonoids and essential oils that possess beneficial bioactivities for human health, it is considered to be agricultural waste.[2] Thus, the utilization of the *C. grandis* peel for the manufacture of natural products is an interesting topic that is related to pharmaceutical and environmental industries.

Naringin is a natural flavonoid compound; naringenin-7-*O*-glycoside (Fig. 1) is responsible for the bitter taste of *C. grandis* fruits. The medicinal value of naringin has been majorly investigated for its antioxidant, anti-inflammatory, and antimicrobial functions. The pharmaceutical applications of naringin can be used to treat various diseases, such as: obesity, diabetes, and heart disease.[3,4] The biological activities of *C. grandis* essential oil, including anti-inflammatory, antibacterial, and cytotoxicity, are considered for commercial applications such as perfume, cosmetic, and medical industries. The main composition of the essential oil is well-known as

[a]*Institute of Chemical Technology, Vietnam Academy of Science and Technology, 1A, TL29, District 12, Ho Chi Minh City, Vietnam. E-mail: maithanhchi@yahoo.com.vn; ntdanh@ict.vast.vn*

[b]*Graduate University of Science and Technology, Vietnam Academy of Science and Technology, 18 Hoang Quoc Viet, Cau Giay, Hanoi, Vietnam*

[c]*Institute of Applied Sciences, HUTECH University, 475A Dien Bien phu Street, Ward 25, Binh Thanh District, Ho Chi Minh City, Vietnam*

[d]*Faculty of Chemical Engineering, Industrial University of Ho Chi Minh City, Ho Chi Minh City 71420, Vietnam. E-mail: trannguyenminhan@iuh.edu.vn*

[e]*Department of Safety Engineering, Dongguk University, 123 Dongdae-ro, Gyeongju-si 780714, Gyeongsangbuk-do, Republic of Korea*

† Electronic supplementary information (ESI) available. See https://doi.org/10.1039/d2ra04068a

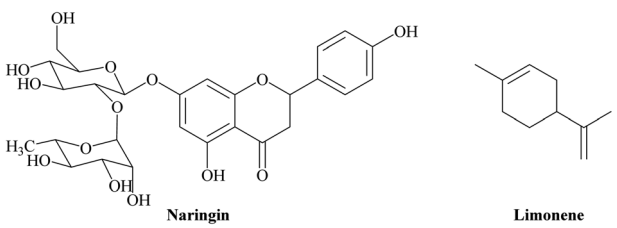

Fig. 1 Chemical structure of naringin and limonene.

monoterpene compounds, with an abundant content of limonene (Fig. 1).[5]

Despite the increasing demand for *C. grandis* essential oils and naringin for human health applications, the lack of economical and environmental-friendly extraction methods has induced the preclusion of commercial development of these natural products. Thus, the enhancement of effective and safe extraction methods is of interest to the market for the products for human health benefits. The *C. grandis* peel is a good source of essential oils and naringin—up to 2% [6] and 3%,[7] respectively. However, most of the extractions were investigated using a common heating extraction, organic solvents, and enzymatic methods. Regarding the biological property of natural products and environmental concerns, the alternative extraction technique using supercritical CO_2 has been of particular interest.[8] Our previous report pointed out that the supercritical CO_2 assisting the extraction could further enhance the efficiency and property of the essential oil compared to the ordinary extraction methods.[9] Quispe-Fuentes *et al.*[10] used supercritical CO_2 and ethanol for the extraction of oils that contain the major content of phenolics. Su *et al.* extracted 45 organic compounds from five different pomelo cultivars using the supercritical CO_2 method.[11] Moreover, the supercritical CO_2 technique has been effectively used for the extraction of essential oils and naringin from other genus citrus.[12–15] The content of naringin obtained in orange, tangerine and lemon peel extracts using the supercritical CO_2 technique was determined to be 35.26, 44.05 and 19.86 mg g^{-1}, respectively.[16] However, to the best of our knowledge, the extraction of both essential oil and naringin, when using supercritical fluid techniques, is rarely reported and any further bioactivity research for them has not yet been evaluated.

A molecular docking model was developed to predict the most stable binding conformation of ligand to a protein or enzyme and test for its QSAR model. It was developed based on a new scoring function that calculates the change of free Gibbs energy and the inhibition constant by using the Lamarckian model of genetics. There are three principal research methods, including the Monte Carlo simulated annealing, the traditional genetic algorithm, and the Lamarckian genetic algorithm. The Autodock and Lamarckian genetic algorithm were used to prove that the molecular docking model is valid.[17] This method has successfully predicted many biological activities *in silico*, such as antimicrobial activity,[18] SARS-CoV-2 resistance of compounds in garlic essential oil,[19] anticancer,[20] inhibition α-glucosidase enzyme,[21] antioxidant,[22] anti-inflammatory,[23] tyrosinase enzyme inhibition,[24] interactions between protein and nanoparticles[25] and acetylcholinesterase inhibition.[26] The validation of the molecular docking model was evaluated by the RMSD value,[27] while the strengths of ligand interactions between ligand and target enzyme or protein were performed by the MD method.[28] Some docking programs and many scoring functions were used to assess the critical docking programs and Scoring Functions.[29] Some protein data bank identifications were classified *via* protein–ligand complexes for docking.[30] Although there are many kinds of molecular docking models, very few report utilising the *in silico* docking model to explain the biological activities of natural products.

In this work, the supercritical CO_2 technique was used to extract essential oil and naringin from *Citrus grandis* peels and their *in vitro* antimicrobial activity, as well as evaluating the *in silico* molecule docking model.

2. Experimental

2.1. Materials

Chemicals, including DMSO, NaOH, and anhydrous Na_2SO_4, were purchased from Acros Co. (Belgium) and ethanol was purchased from Chemsol Co. (Vietnam). Waste *Citrus grandis* peels were collected in BenTre Provine, Vietnam. The peels were cut with to a particle size of 1–2 mm using a slicer machine. Deionised water was used throughout the experiment.

2.2. Extraction methods of essential oils

2.2.1. Conventional hydro-distillation. *C. grandis* peels (100 g) and distilled water (500 ml) were put into a round-bottom flash and connected with a Clevenger apparatus. The samples were refluxed for 4 hours. Eventually, the essential oil was separated and dried with anhydrous Na_2SO_4. Dry hydro-distillation essential oil (HDEO) was collected as a pale oil.

2.2.2. Supercritical CO_2 extraction. The supercritical CO_2 assisting the extraction was carried out following the previous report.[9] Briefly, the peels (500 g) were added into a high-pressure vessel (2000 ml) and connected with a separator operating up to 200 bar. The extraction was conducted with the flow rate for the supercritical CO_2 at 0.5 g min^{-1} at 40 °C and 100 bar. After reducing the pressure, the CO_2 gas and essential oil (SCEO) were separated from each other. Both the HDEO and SCEO were stored at 0–5 °C for further studies.

2.3. Extraction of naringin

Naringin was extracted using supercritical CO_2 and ethanol as a co-solvent. The essential oil required 100 g of peels in 200 ml of different concentrations of ethanol solution (50, 80, 90, and 96%) and put into a stainless-steel extraction cell – 0.5 L. Extraction conditions were optimized with changes in temperature (30–70 °C), pressure (100–130 bar) and time (1–4 hours); the extract was evaporated to remove the ethanol and give the residue. 300 ml of NaOH solution (1 M) was then added to the residue to remove the polysaccharides and impurities. The solid was washed with ethanol (100 ml × 3) and oven-dried at 60 °C; the collected product was dissolved in 200 ml of H_2O at 75 °C for 10 minutes. After the drying step, the hot mixture was filtered, 100 ml of ethanol solution (20%) was then added into the extraction. The solution's pH was verified to be 4, after that, it was cooled at 15 °C for 24 hours. The pure naringin was filtered and dried at 50 °C for 6 hours. The product, after this final drying process, was comprised of two epimers at position C-2 and was a white amorphous powder which could be observed in ^{1}H and ^{13}C NMR spectra. $[\alpha]_D^{20} = -82.4°$ (ethanol, 1 g ml^{-1}). ESI-HRMS (*m*/*z*): 579.1714 $[M + H]^+$ calcd for $C_{27}H_{31}O_{14}$ ($[M + H]^+ = 579.1714$).

2.3.1. 2*S*-Naringin.[31] ^{1}H-NMR (600 MHz, DMSO-d_6, δ ppm): 5.49 (1H, dd, 13.2; 3.0, H-2), 2.72 (1H, dd, 13.2, 3.0, H-3ax), 3.14–

3.17 (1H, m, H-3eq), 6.08 (1H, d, 2.4, H-6), 6.10 (1H, d, 2.4, H-8), 7.32 (1H, d, 8.4, H-2′, H-6′), 6.79 (1H, d, 8.4, H-3′, H-5′), 5.13 (1H, d, 7.8, H-1″), 3.39 (1H, m, H-2″), 3.41 (1H, m, H-3″), 3.19 (1H, m, H-4″), 3.40 (1H, m, H-5″), 3.40 (1H, m, H-6a″), 3.65 (1H, m, H-6b″), 5.09 (1H, d, 1.8, H-1‴), 3.17 (1H, m, H-2‴), 3.67 (1H, m, H-3‴), 3.30 (1H, m, H-4‴), 3.69 (1H, m, H-5‴), 1.14 (1H, d, 6.0, H-6‴), 12.04 (1H, s, 5-OH), 9.64 (1H, s, 4′-OH). ^{13}C-NMR (150 MHz, DMSO-d_6, δ ppm): 78.6 (C-2), 42.0 (C-3), 197.2 (C-4), 163.0 (C-5), 96.3 (C-6), 164.7 (C-7), 95.1 (C-8), 162.8 (C-9), 103.3 (C-10), 128.6 (C-1′), 128.4 (C-2′, C-6′), 115.2 (C-3″, C-5″), 157.8 (C-4″), 97.3 (C-1″), 77.1 (C-2″), 76.9 (C-3″), 71.8 (C-4″), 76.1 (C-5″), 60.4 (C-6″), 100.4 (C-1‴), 69.6 (C-2‴), 70.4 (C-3‴), 70.5 (C-4‴), 68.3 (C-5‴), 18.0 (C-6‴).

2.3.2. 2*R*-Naringin.[31] ^{1}H-NMR (600 MHz, DMSO-d_6, δ ppm): 5.51 (1H, dd, 12.6; 3.0, H-2), 2.73 (1H, dd, 13.8, 3.0, H-3eq), 3.18–3.21 (1H, m, H-3ax), 6.09 (1H, d, 2.4, H-6), 6.11 (1H, d, 2.4, H-8), 7.33 (1H, d, 8.4, H-2′, H-6′), 6.80 (1H, d, 8.4, H-3′, H-5′), 5.14 (1H, d, 7.8, H-1″), 3.39 (1H, m, H-2″), 3.41 (1H, m, H-3″), 3.19 (1H, m, H-4″), 3.40 (1H, m, H-5″), 3.40 (1H, m, H-6a″), 3.65 (1H, m, H-6b″), 5.09 (1H, d, 1.8, H-1‴), 3.17 (1H, m, H-2‴), 3.67 (1H, m, H-3‴), 3.30 (1H, m, H-4‴), 3.69 (1H, m, H-5‴), 1.14 (1H, d, 6.0, H-6‴), 12.05 (1H, s, 5-OH), 9.65 (1H, s, 4′-OH). ^{13}C-NMR (150 MHz, DMSO-d_6, δ ppm): 78.8 (C-2), 42.1 (C-3), 197.3 (C-4), 163.0 (C-5), 96.4 (C-6), 164.9 (C-7), 95.2 (C-8), 162.9 (C-9), 103.4 (C-10), 128.6 (C-1′), 128.5 (C-2′, C-6′), 115.2 (C-3″, C-5″), 157.9 (C-4″), 97.4 (C-1″), 77.1 (C-2″), 76.8 (C-3″), 71.8 (C-4″), 76.2 (C-5″), 60.4 (C-6″), 100.5 (C-1‴), 69.6 (C-2‴), 70.4 (C-3‴), 70.5 (C-4‴), 68.3 (C-5‴), 18.0 (C-6‴).

The extraction yield (%) was calculated as the weight of obtained naringin over the weight of dry peels used at the beginning.

$$\text{Extraction yield (\%)} = \frac{\text{mass of naringin}}{\text{mass of dry peels}} \times 100\% \quad (1)$$

2.4. Measurement

Gas chromatography (GC) and Gas chromatography-mass spectrometer (GC-MS) measurements of EOs were carried out, as stated in the previous report.[32] Briefly, the EOs (25 μL) were dissolved in hexane (1 ml) and analysed on GC (Agilent 6890 N) coupled with HP-5MS Capillary Column (30.0 length × 0.25 mm i.d. × 0.25 μm film thickness). The retention index was calculated based on the standard sample containing homologous series of *n*-alkanes (C_8–C_{30}, Sigma Co.). To identify the essential oils, their retention index was compared with the published data. For the measurement of infrared spectra, the A BRUKER EQUINOX 55 IR spectrophotometer was used during this process. ^{1}H and ^{13}C NMR (BRUKER AVANCE 500 NMR spectrometer) analysis was recorded with DMSO-d_6 as the solvent and tetramethyl silane (TMS) played the role of the internal standard. The optical rotation was measured on the A. Kruss polarimeter P8000-T using ethanol solvent. The HRMS spectrum was measured on the Agilent 6200 series TOF.

2.5. Antibacterial assay

2.5.1. Disk diffusion. The essential oil and naringin were screened for their inhibition activity against three Gram-positive bacteria, *Staphylococcus aureus* ATCC 29213, *Streptococcus pyogenes* ATCC and *Streptococcus pneumoniae* ATCC 29212, three Gram-negative bacteria *Moraxella catarrhalis* ATCC, *Pseudomonas aeruginosa* ATCC 27853, and *Haemophilus influenzae* ATCC 33533, and three fungi, *Trichophyton mentagrophytes*, *Trichophyton rubrum*, and *Microsporum gypseum*, using the disk diffusion method.[28] Drugs including ampicillin and fluconazole, at a concentration of 1.0 mg ml^{-1} were chosen to be the standard drugs for positive standards of the bacteria and fungi, respectively. The microbial test organisms were prepared in LB broth for 24 hours at 37 °C and gel plates for the bacteria and fungi were prepared in Mueller–Hinton Agar (MHA) and Potato Dextrose Agar (PDA), respectively. Each strain was swabbed uniformly into the individual plate using sterile cotton swabs, while the MHA/PDA were covered with paper dishes (diameter 6 mm). The SCEO at a concentration of 10 mg ml^{-1} or naringin at different concentrations—from 6.25 to 100 μM were taken equally at 30 μL. The positive control at 30 μL was put into a separate paper disk for each microbial strain. After incubation at 25 °C for 24 hours (bacteria) or 37 °C for 48 hours (fungi), the measuring of the inhibited zone was then conducted.

2.5.2. The macro-broth dilution assay. The active entries were used to identify the lowest concentration MIC value that inhibited the growth of bacteria in the *in vitro* test method. The SCEO was diluted two-fold in dimethyl sulfoxide DMSO (0.05%) to afford different concentrations, then the samples were incubated in a bacterial solution media culture. Informatively, the suitable temperature for bacteria was 37 °C and the incubation was carried out for 24 hours.[33]

2.6. *In silico* molecular docking model for anti-microbial activities

The *in silico* docking model for essential oil and naringin was conducted by a general procedure in Scheme 1. For essential oil, D-limonene docked to a receptor of bacterium, *M. catarrhalis*, code 4ZQG: PDB. The active centre of bacterium *M. catarrhalis* was determined at coordinates of $X = -2.685$, $Y = -1.666$, $Z = -32.403$. The grid parameters were installed by spacing and the numbers of points in the (X, Y, Z) axis, which were 0.5 Å and (50, 50, 50), respectively in dock.gpf file. The number of models was 200 models, while the results of the docking model were calculated by the Discovery Studio 2021 client and Molegro Molecular Viewer. Additionally, the validations of the models were calculated by the PyMOL package in values of RMSD, as reported 30. The ADMET model, or drug-likeness of the compound, were determined based on ADMETlab 2.0—an online platform solution.[34]

The naringin ligand was docked to one receptor, an enzyme with the code 2VF5 from the protein data bank (PDB file). As the chosen enzyme, 2VF5 was determined to be the catalyst for the synthesis of glucosamine-6-phosphate (GlcN-6-P). Hence, the short-time inhibition of GlcN-6-P synthase harmed and restrained the growth of the fungal cells, or fungi.[35] The active centre of 2VF5: PDB was detected at coordinates of ($X = 26.579$, $Y = 22.731$, $Z = 8.113$). The grid parameters were set up in dock.gpf file by the spacing of 0.5 Å, the numbers of points in (X, Y, Z) axis of (50, 50, 50), respectively, and the centre of grid box

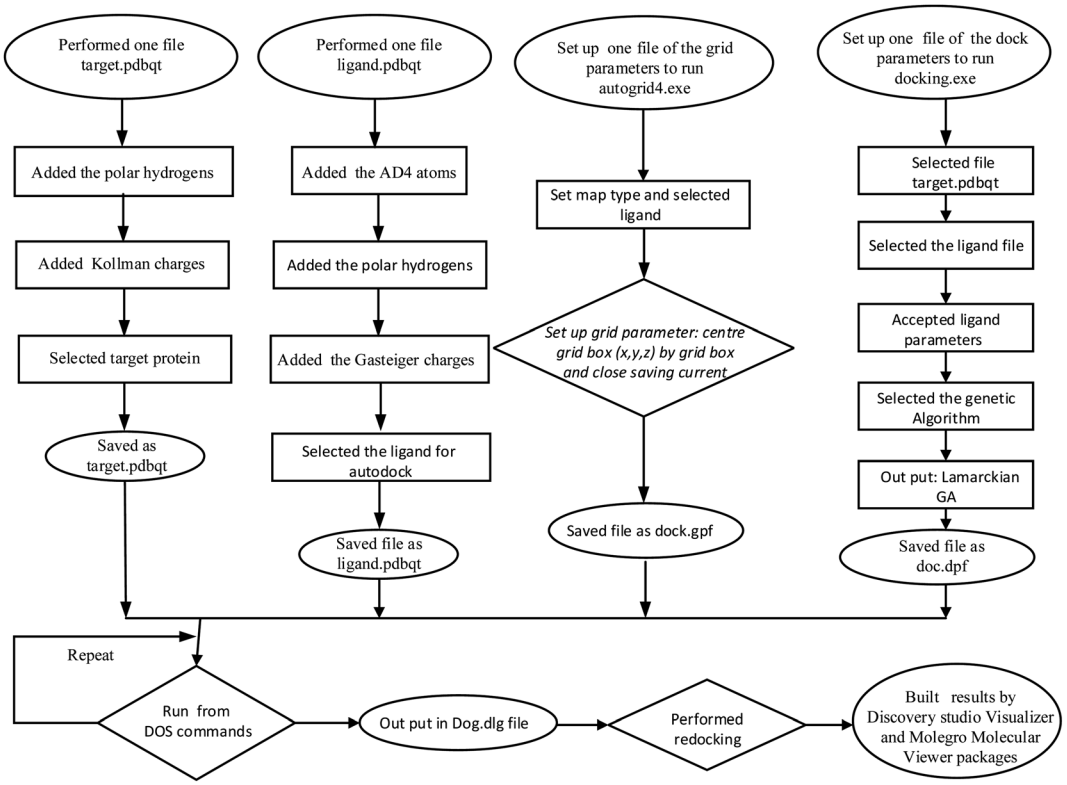

Scheme 1 The general procedure for the docking of naringin or the main components of the essential oil to enzyme 2VF5 or bacterium: 4ZQG: PDB.

of $X = 26.579$, $Y = 22.731$, $Z = 8.113$. The input and output were installed by a generic algorithm with 200 models and Lamarckian in dock.dpf file, respectively.

2.7. Molecular dynamics simulation of the best docked model complex

Based on docking results, molecular dynamics (MD) simulation of naringin was performed on the selected lowest energy and the best docking complex using the GROMACS 2020 series package (gromacs.org) with the CHARMM force field (**https://www.charmm.org**). The SwissParam server was used to generate ligand topology files (swissparam.ch). Three-point transferable intermolecular potential (TIP3P) was chosen as a solvent model for protein–ligand complexes (triclinic water box with a size of 50 × 75 × 70 Å).[36] Before the minimization process, the charge system was applied to neutralize by the addition of 0.15 M NaCl at constant temperature (300 K) and pressure (1.0 bar). Energy minimization was performed using the steepest descent approach for the protein–ligand complex. In the final step, MD simulation with 100 ns was performed for compound naringin, pose 60 and receptor, crystal structure of enzyme 2VF5: PDB in periodic boundary condition and 1000 frames were used in each simulation. Findings such as Root Mean Square Deviation and Fluctuation (RMSD/F), hydrogen bond counting, and radius of gyration (R_g) were analyzed using Xmgrace software (plasma-gate.weizmann.ac.il/Grace) and other tools such as OriginLab and VMD.

3. Results and discussion

The application of the green technique is particularly important for the production of natural compounds in pharmaceutical fields. In this work, the supercritical CO_2 technique was applied to extract the essential oil from waste *C. grandis* peel source, followed by producing naringin using the EO spent *C. grandis* peels. For detailed information, the study strategy is fully provided in Scheme 2. To confirm the efficiency of the extraction, the hydro-distilled essential oil was used as a reference sample. The chemical composition of essential oils was identified using GC-MS spectra, then compared with the reference. The supercritical CO_2 extraction of naringin was optimized within experimental conditions; then, its purity and structure were identified using 1D and 2D NMR spectra. The pharmaceutical applications of both SCEO and naringin were evaluated *via* antimicrobial activity as well as a docking study.

3.1. Volatile compositions, antimicrobial activity, and docking study of essential oils

3.1.1. Volatile compositions. The chemical components of SCEO were determined using GC-MS spectra, with HDEO as a reference sample. The percentage of volatile compounds was determined by the area integration from GC and GC-MS spectra and the values were expressed in retention index and percentages. The spectra are shown in Fig. 2 while relative compositions are listed in Table 1. There was a significant difference in

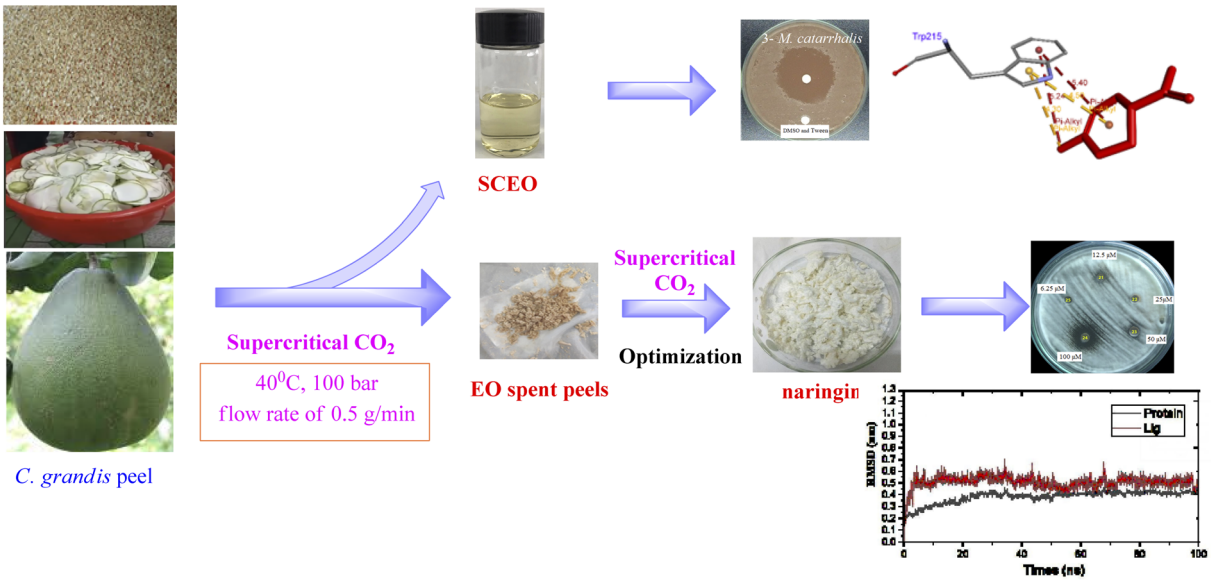

Scheme 2 Study strategy for supercritical CO_2-assisted extraction of essential oil and naringin and their applications in the pharmaceutical field.

their chemical components. Twelve identifiable compounds, with a total of 99.04%, were found in HDEO, hence, the majority were determined to be monoterpene (98.53%), including hydrocarbons (91.60%), and alcohols (61.93%). Hydrocarbon monoterpenes in HDEO consist of D-limonene (87.60%), β-pinene (1.51%), α-phellandrene (1.13%), α-pinene (0.90%), *o*-cymene (0.46%) while alcohol monoterpenes include (*Z*)-linalool oxide (2.30%), α-terpineol (1.92%), linalool (1.36%), (*E*)-linalool oxide (0.94%) and 4-terpineol (0.38%). Conversely, SCEO only contains D-limonene, well-known as a natural hydrocarbon terpene that possesses valuable bioactivities such as antibacterial,[37,38] anti-inflammation,[39] and anticancer.[40] It is clearly proved that supercritical CO_2 can enhance the extraction of *C. grandis* peels to obtain pure D-limonene. Additionally, the recent reports also showed that supercritical CO_2 extraction could improve the content of major volatile compounds in essential oils, depending on relative extraction conditions.[9,41]

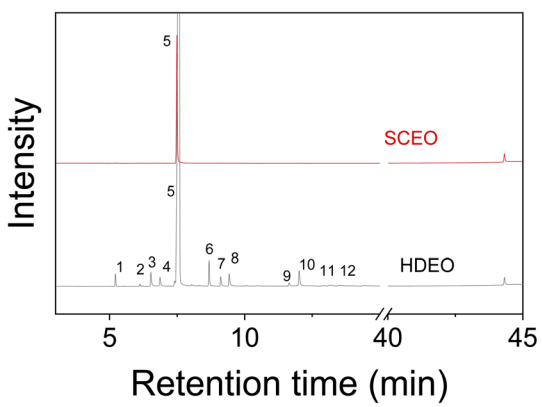

Fig. 2 GC-MS spectra of *C. grandis* essential oils extracted by hydro-distillation (HDEO) and Supercritical CO_2 (SCEO) methods.

3.1.2. Antimicrobial activities of essential oil. The *in vitro* antibacterial activities of SCEO were tested against six bacterial strains, *Pseudomonas aeruginosa* (P. a), *Staphylococcus aureus* (S. a), *Moraxella catarrhalis* (M. c), *Streptococcus pyogenes* (S. py), *Streptococcus pneumoniae* (S. pn), and *Haemophilus influenzae* (H. i) at a concentration of 100 mg ml^{-1} using the disk diffusion method.[43,44] The results showed that SCEO exhibited multiple inhibitions against different strains (Fig. 3). Indeed, the sample

Table 1 Chemical composition of *C. grandis* essential oils extracted by hydro-distillation and supercritical CO_2 methods

				% GC		
No.	Compounds	RI[a]	RI[b]	HDEO	SCEO	Method
1	α-Pinene	932	927	0.90	—	RI, MS
2	β-Pinene	974	980	1.51	—	RI, MS
3	α-Phellandrene	1003	996	1.13	—	RI, MS
4	*o*-Cymene	1014	1015	0.46	—	RI, MS
5	D-Limonene	1028	1022	87.60	95.66	RI, MS
6	(*Z*)-Linalool oxide	1066	1061	2.30	—	RI, MS
7	(*E*)-Linalool oxide	1076	1077	0.94	—	RI, MS
8	Linalool	1090	1089	1.39	—	RI, MS
9	4-Terpineol	1170	1166	0.38	—	RI, MS
10	α-Terpineol	1187	1180	1.92	—	RI, MS
11	β-Caryophyllene	1413	1406	0.31	—	RI, MS
12	α-Caryophyllene	1438	1439	0.10	—	RI, MS
Monoterpenes						
Hydrocarbons				91.60	95.66	
Alcohols				6.93	—	
Sesquiterpenes						
Hydrocarbons				0.41	—	
Not identified				1.07	4.34	

[a] Retention index was collected from ref. 42 and NIST database. [b] Retention index was calculated from the experimental data.

did not inhibit three bacterial strains (P. a, S. a, and H. i) but it had excellent inhibition against M. c, S. py and S. pn at a concentration of 100 mg ml^{-1} with an inhibition zone of 44 mm, 14 mm and 18 mm, respectively. The high antibacterial activity of SCEO against S. py and S. pn was similar to the essential oils that contained an abundant content of D-limonene as previous reports stated.[45,46] It was also noted that the bioactivity of SCEO against M. c strain was higher than that of ampicillin at 1.0 mg ml^{-1}.

MIC values of SCEO against bacteria M. c, S. py, and S. pn were determined *via* the dilution method. The test concentrations were used for strain M. c in the range of 0.06–0.5 mg ml^{-1} while the concentration series for the inhibition of both S. py and S. pn were performed in the range of 0.25–2.0 mg ml^{-1}, followed by plotting the antibacterial activity in Fig. 4A, while test images are shown in Fig. 4B. The result was identified and showed that the MIC values of SCEO against all bacteria strains were very low. MIC values inhibited both strains, S. py and S. pn, were determined to be 1.0 mg ml^{-1} while the value of M. c inhibition was low, at a value of 0.25 mg ml^{-1}. These values showed a better activity than was found for essential oils, with an abundant content of D-limonene reported previously. Wang *et al.*[47] found MIC of Citrus medica essential oil with D-limonene of ~50% against strain S. pn was 24 mg ml^{-1}. Salama[46] showed that *Myoporum acuminatum* essential oil that contained approximately 34% of D-limonene possessed MIC value against S. pn at about 3.0 mg ml^{-1}. Doughari and Bazza showed essential oil isolated from *Citrus*

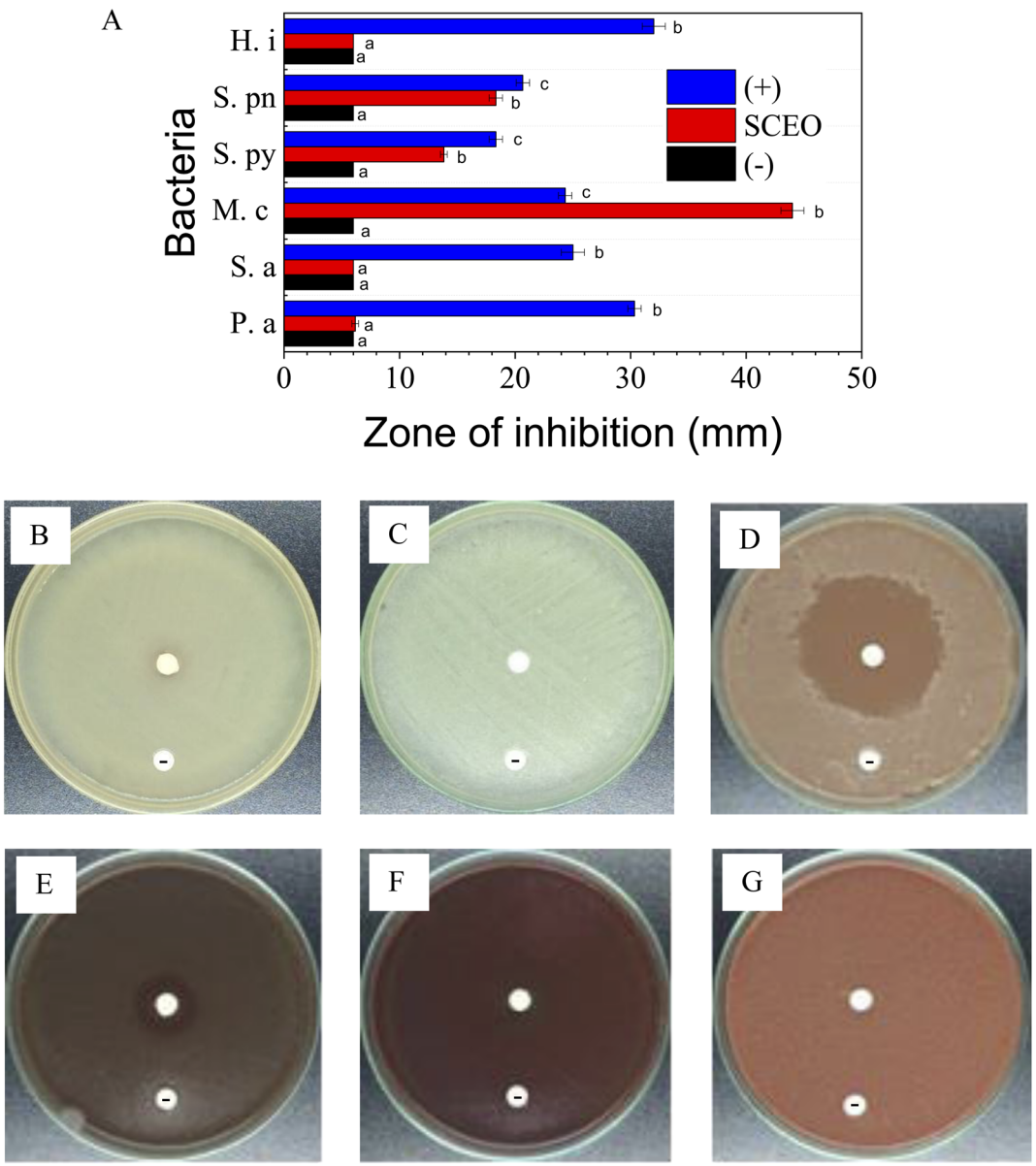

Fig. 3 The plot of antibacterial activity with different letters indicating significant differences at $p < 0.05$ (A) and test images of SCEO performed at a concentration of 100 mg ml^{-1} against different bacteria P. a (*Pseudomonas aeruginosa*) (B), S. a (*Staphylococcus aureus*) (C), M. c (*Moraxella catarrhalis*) (D), S. py (*Streptococcus pyogenes*) (E), S. pn (*Streptococcus pneumoniae*) (F), H. i (*Haemophilus influenzae*) (G). DMSO, and ampicillin (1 mg ml^{-1}) were used as negative and positive controls, respectively.

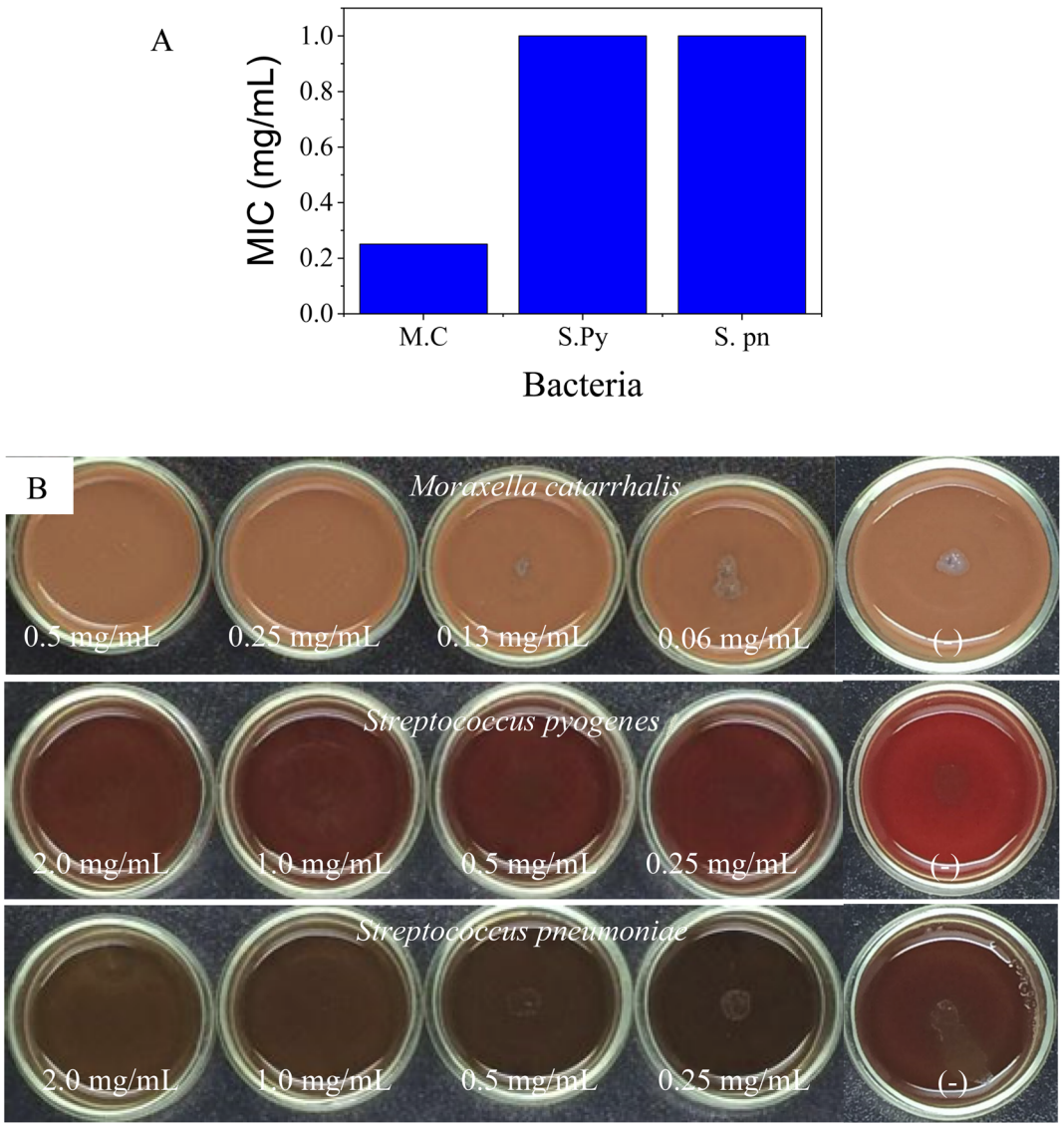

Fig. 4 (A) The plots of MIC values of SCEO against bacteria M. c (*Moraxella catarrhalis*), S. py (*Streptococcus pyogenes*), and S. pn (*Streptococcus pneumoniae*), and (B) photos of SCEO for the antibacterial test against bacterial strains.

sinensis possessed MIC of 200 mg ml^{-1} against strain S. py. Meanwhile, the essential oils containing an abundant content of D-limonene were rarely used for testing against strain M. c, which may cause infections of the eye, middle ear, and central nervous system of humans.[48]

3.1.3. *In silico* docking study of D-limonene. Due to high antibacterial activity of SCEO against *M. catarrhalis* strain, this bacterium was selected to calculate *in silico* molecular docking model with PDB code 4ZQG. The major component of the essential oil, D-limonene ligand, was docked to 4ZQG: PDB. Pose 66 – a ranked pose of ligand D-limonene or the best stable conformation ligand was docked to active site of protein of M. c with the values of Free Energy of binding and inhibition constant of −6.02 kcal mol^{-1} and 38.71 μM, respectively. This pose made ligand interactions to Trp 125 of B chain. Those interactions were named two π-alkyl interactions (red colour) from phenyl ring of Tyr215 to pose 66 at distances of 5.40 and 5.24 Å, respectively; the others were two π-alkyl (orange color) interactions from active atoms on indole ring of Trp 215 to active atom on pose 66 at distances of 4.30 Å and 4.50 Å, respectively. As shown in Fig. 5A, the best stable conformation of ligand fosmidomycin docked to crystal structure of *M. catarrhalis* bacterium showed the binding free energy of −3.34 kcal mol^{-1} and inhibition constant of 38.71 mM. As shown in Fig. 5B, pose 18 interacted with residual amino acid of chain B (Arg 292) showed hydrogen bonding, salt bridge and electrostatic interaction from Arg 292 to negative oxygen atoms of phosphate group at distances of 5.22 Å, 6.77 Å and 6.45 Å, respectively. A charge repulsion from Arg 292 to positive phosphorus atom was determined at distance of 6.37 Å. Moreover, a carbon hydrogen interaction formed from Cys 162 of chain B to oxygen atom of carbonyl group. The study on thermodynamic site showed that pose 66 interacted with crystal structure of protein 4ZQG better than that of pose 18 (fosmidomycin). In

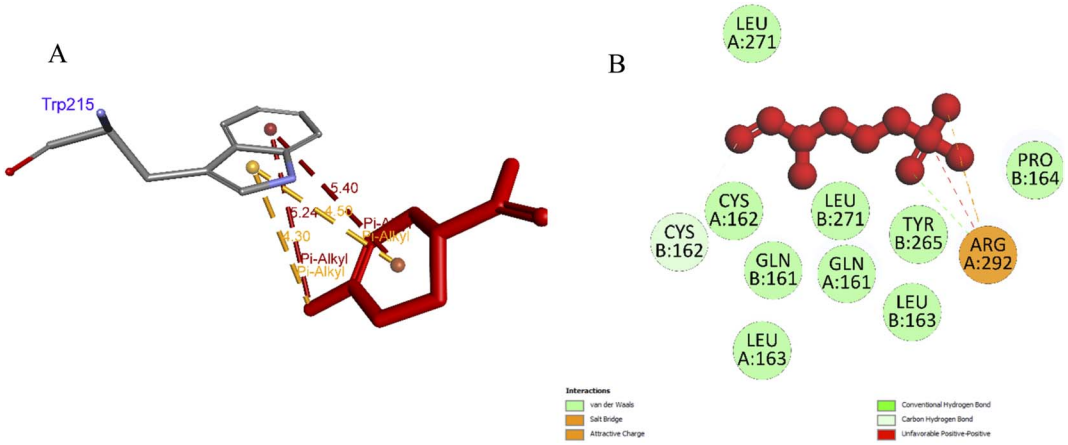

Fig. 5 (A) Pose 66 docked to residual amino acid Trp 215 of 4ZQG: PDB; (B): small ligand, pose 18 (fosmidomycin) in crystal structure of 4ZQG: PDB was redocked to one crystal structure of protein 4ZQG: PDB.

ligand interactions, pose 66 and pose 18 well interacted with Trp 215 and Arg 292 or Cis 162, respectively. The RMSD of pair pose (pose 66 and pose 18) was not conducted because the atomic alignment was failed.

The pharmacokinetic model of D-limonene was predicted in Tables S1–S8.† As seen in Table S1,† the physicochemical properties of compound D-limonene were detected in a permission range. The significant parameters were TPSA, log *S*, log *P*, and log *D*. The medicinal parameters were determined as shown in Table S2,† most of them were in range as Lipinski Rule, Sascore, Fsp^3, Npscore, PAINS, ALARM NMR, BMS, and Chelator Rule. The absorption properties were detected in range as HIA, Caco-2 permeability in Table S3.† As shown in Table S4,† compound D-limonene was proved to have good distribution properties, except for BBB Penetration parameter while the drug metabolism, drug excretion, drug toxicity, and toxicophoric rules were indicated in Tables S5–S8,† respectively. They were confirmed as a drug-likeness. Therefore, compound D-limonene was indicated to be the potential drug properties.

3.2. Extraction, antimicrobial activity, and docking study of naringin

3.2.1. Extraction. Extraction of naringin from essential oil spent *C. grandis* peels using supercritical CO_2 and ethanol solution as a co-solvent was strongly dependent on the experimental conditions, which were optimized *via* the evaluation of obtained yields (eqn (1)). In this work, the extraction conditions, including ethanol concentration, pressure, temperature and time were investigated. The data was then plotted in Fig. 6. The result showed different trends in changes in extraction parameters, indicating that the supercritical CO_2 extraction efficiency of naringin was strongly dependent on the experimental conditions.

Extraction performance is strongly influenced by ethanol concentrations, as clearly observed in Fig. 6A. The extraction yield was seen to be 2.4% with an ethanol concentration of 50%. The yield was significantly improved when the ethanol concentration used was 80%. However, no significant change in the extraction yield was seen when higher concentrations of ethanol were observed. Due to the requirement of production cost efficiency, the concentration of ethanol solution (80%) was used for naringin extraction.

For the effect of pressure, the extraction was investigated in a range from 100 to 130 bar. The pressure-dependent extraction of naringin is obviously seen in Fig. 6B. The extraction yield obtained only 2.5% at the low pressure (100 bar) and increased proportionally with the pressure. The maximum yield achieved (3.8%) was at a pressure of 120 bar and did not change with a higher pressure (130 bar).

Extraction temperature was performed in a range from 30 to 70 °C (Fig. 6C). The result indicated that the extraction yield was ineffective at a low temperature (30 °C) while a high temperature (more than 50 °C) insignificantly affected the extraction of

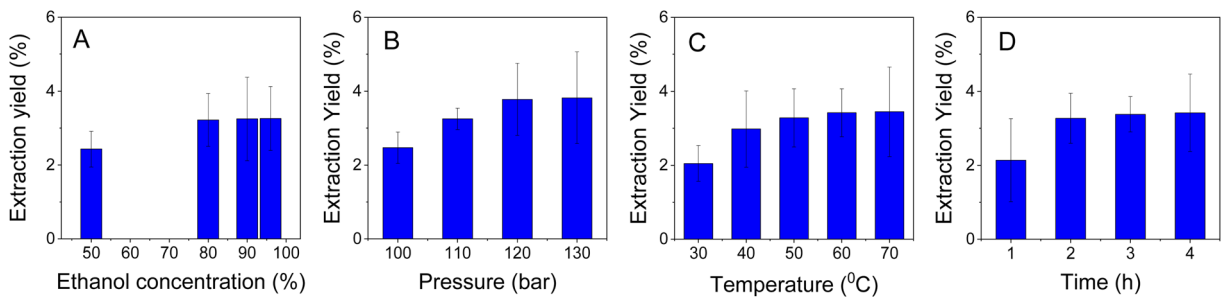

Fig. 6 Influence of conditions on naringin extraction yields: (A) ethanol concentration; (B) pressure; (C) temperature; and (D) time.

naringin. Thus, the optimum temperature was determined to be 50 °C, with a yield of 3.3%.

The time-dependent extraction of naringin was optimized at a range within 1 to 4 hours. A low extraction efficiency was observed for the initial hour and the higher yields (3.3%) were obtained after 2 hours of extraction. Thus, the result given showed that the best experimental condition for supercritical CO_2-assisted extraction of naringin was carried out at a concentration of 80% ethanol solution, 120 bar pressure, a temperature of 50 °C and a time of 2 hours. The structure of the obtained compound was clearly identified as naringin by ^{1}H and ^{13}C NMR spectra. From the data of 2D NMR (HSQC, COSY and HMBC), the structure of the obtained naringin was confirmed to be an epimer mixture at position C-2.

3.2.2. Antibacterial activity of naringin. The antibacterial activity of naringin was also evaluated against six bacterial strains, including S. a, S. pn, S. py, P. a, M. c, and H. i at different concentrations in the range of 6.25–100 μM. The data is plotted in Fig. 7. The results showed that naringin exhibited moderate activity against all tested bacteria and its activity was gradually reduced with respect to a decrease in the sample concentrations. The zones of inhibition were found to be in the range of 10–15 mm at the highest test concentration of 100 μM while the largest inhibition was found to be 15 mm for the test of S. a strain. The MIC values were plotted in Fig. 7B. The data showed that MIC values of naringin against three strains of S. a, S. pn and H. i (6.25 μM) were much lower than the values of three strains of S. py, P. a and M. c (25 μM). The result indicated that the antibacterial activity of naringin is strongly dependent on the bacterial strains. It was thought to be due to the difference between the membrane and cell wall structure.[49]

3.2.3. Antifungal activity of naringin. Because naringin is commonly used in the inflammatory, therapeutic, and cosmetic industries, its antifungal activities were screened against *Trichophyton rubrum* (T. r), *Trichophyton mentagrophytes* (T. m), and *Microsporum gypseum* (M. g) fungi, which are well known as the most common cause of infection on the skin of animals and humans. The investigation of antifungal activity was carried out at various concentrations from 6.25 to 100 μM, as seen in Fig. 8. The result showed that naringin inhibited good activity against all test fungi at a concentration of 100 μM, with inhibition zones in the range of 18–21 mm. Among the fungal strains, naringin inhibited well against two strains, T. m and M. g, which was confirmed with MIC values of 6.25 and 12.5 μM, respectively. The strain, T. m, is a common fungus that causes ringworm in companion animals and tinea infections in humans while the strain, M. g, is a dermatophyte that infects the skin of mammals. The good inhibition of naringin against these fungal strains is particularly important and suggests a potential natural drug for the treatment of microbial infections.

3.2.4. *In silico* docking study of naringin. Among its antimicrobial activities, naringin indicated high *in vitro* inhibition activity against fungi, including T. r, T. m, and M. g. To gain insights into the antifungal behaviour of naringin, the *in silico* molecular docking model was performed. The explanation was based on the mechanism of the enzyme inhibition 2VF5: PDB, Glucosamine-6-phosphate synthase enzyme (GlcN-6-P), which was an effective target in antimicrobial chemotherapy. This enzyme participates in the metabolism of hexosamine, such as uridine, 5′-diphospho-*N*-acetyl-D-glucosamine (UDP-GlcNAc) synthesized amino sugars by the biosynthetic process. The UDP-GlcNAc, a key component of the peptidoglycan layer was mostly detected in the bacterial and fungal cell walls. Inactivation of the GlcN-6-P synthase enzyme for a short period is highly harmful to fungal cells.[4] The remarkable results of the docking model of naringin, pose 60 and small ligand (available in enzyme 2VF5), pose 83 were shown in Table S9† and Fig. 9. Pose 60, ligand naringin, ranked pose 60 among docking poses (200

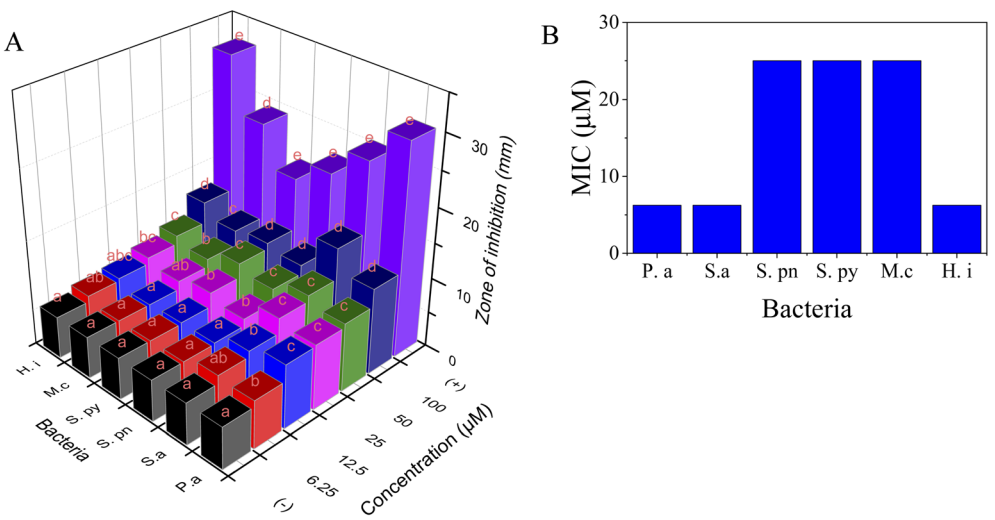

Fig. 7 (A) The antibacterial activity of naringin performed using the dish diffusion method at different concentrations (6.25–100 μM), against different bacteria, P. a (*Pseudomonas aeruginosa*), S. a (*Staphylococcus aureus*), S. pn (*Streptococcus pneumoniae*), S. py (*Streptococcus pyogenes*), M. c (*Moraxella catarrhalis*), H. i (*Haemophilus influenzae*). DMSO and ampicillin (1 mg mL^{-1}) used as negative and positive controls, respectively; and (B) plots of MIC values used for different bacterial strains.

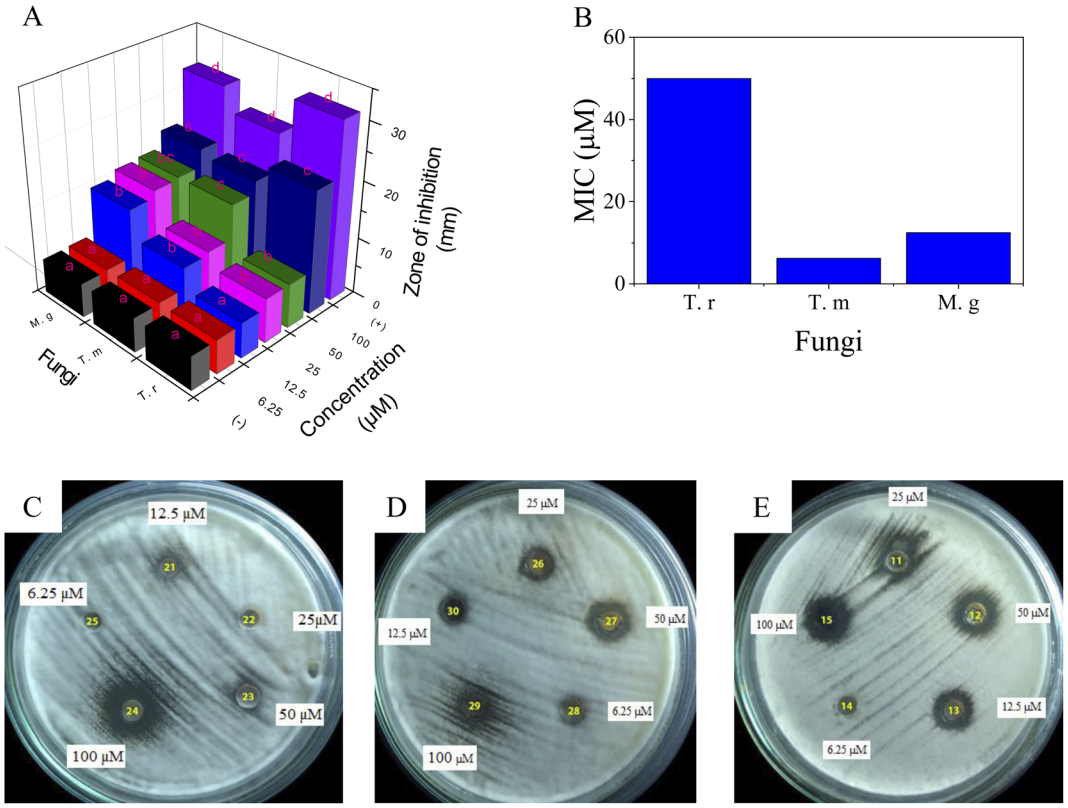

Fig. 8 (A) Plots of the antifungal activity of naringin performed *via* the dish diffusion method at different concentrations (6.25–100 μM) against different fungi, T. r (*Trichophyton rubrum*), T. m (*Trichophyton mentagrophytes*), M. g (*Microsporum gypseum*). DMSO and fluconazole (1.0 mg ml^{-1}) used as negative and positive controls, respectively. (B) Plots of MIC values against fungal strains. Photos of the antifungal activity against (C) *T. rubrum*, (D) *T. mentagrophytes*, and (E) *M. gypseum*.

models) was identified to be the most stable conformation ligand docked to enzyme 2VF5, with the values of Free Gibbs energy and inhibition constant calculated at −5.51 kcal mol^{-1} and 91.22 μM, respectively, as shown in Table S9.† The ranked pose 60 (blue colour) docked to a pocket enzyme 2VF5, as seen in Fig. 9A, and this pose formed four hydrogen bonds from residual active amino acids on 2VF5, such as Gly301, Lys 487, and Ala 496 to oxygen and hydrogen atoms on pose 60 or ligand naringin (Fig. 9B and Table S9†). The interactions were electrostatic or hydrogen or hydrophilic interactions and indicated that the ligand was a hydrophilic molecule. The hydrogen bond, naringin: H–X: Lys 603, was the strongest due to the shortest bond length among the four hydrogen bonds.

The ligand interactions between pose 60 and 2VF5 could be observed on the 2D diagram (Fig. 9C). The results showed that this pose did not have good interaction with enzyme 2VF5. Ligand naringin, pose 60, interacted well with the enzyme because three parts of this pose (capping group, connecting unit, and functional group) were well detected with enzyme 2VF5.[30] The capping group was identified *via* a π–σ interaction, which linked from Leu 484 to the system of π electrons of the aromatic ring. The connecting unit (CU) was shown to have no ligand interaction, and the functional group of pose 60 formed hydrogen bonds from Lys 603, Asn 305, Lys 487 to the hydrogen atom of phenolic hydroxyl groups of phenyl ring, the hydrogen atom of the alcohol group, and the oxygen atom of oxygen heterocyclic, respectively. As shown in Fig. 9D, the ligand map exposed the secondary interactions that formed from active residual amino acids on the enzyme to the active atom on pose 60. They included hydrogen bonds (yellow lines) from Asn 305, Ala 496, Lys 487, and Lys 603 to active atoms on pose 60 and the steric interactions from Tyr 304, Asn 305, Lys 487, Glu 488, Glu 495, Leu 601, and Ala 602. More steric forming around pose 60, the strength of interactions between this pose and the active residual amino acids, were stronger in the processing of a docking pose such as pose 60. The overlap interactions between pose 60 and 2VF5 enzyme were depicted by the violet circles on the atoms of pose 60 and the size of the violet circles were bigger and stronger in the overlapping interactions.

Small ligand in 2VF5 enzyme: ranked pose 83 docked to 2VF5 enzyme as seen in Fig. 9A–G and Table S9.† Pose 83 was the best docking pose among the 200 poses—it docked to active atoms on enzyme 2VF5, with the values of Free Gibbs energy and inhibition constant of −5.38 kcal mol^{-1} and 114 μM, respectively, as shown in Table S9.† Pose 83 formed 13 hydrogen bonds with active residual amino acids of enzymes such as Thr302, Glu 348, Ser 349, Thr 352, Ser 401, Glu 488, Ala 602, and Lys 603 and proved pose 83 had more hydrophilic properties (Fig. 9E). As shown in Fig. 9F, pose 83 did not interact well with the enzyme because the capping group and connecting unit were not identified *via* ligand

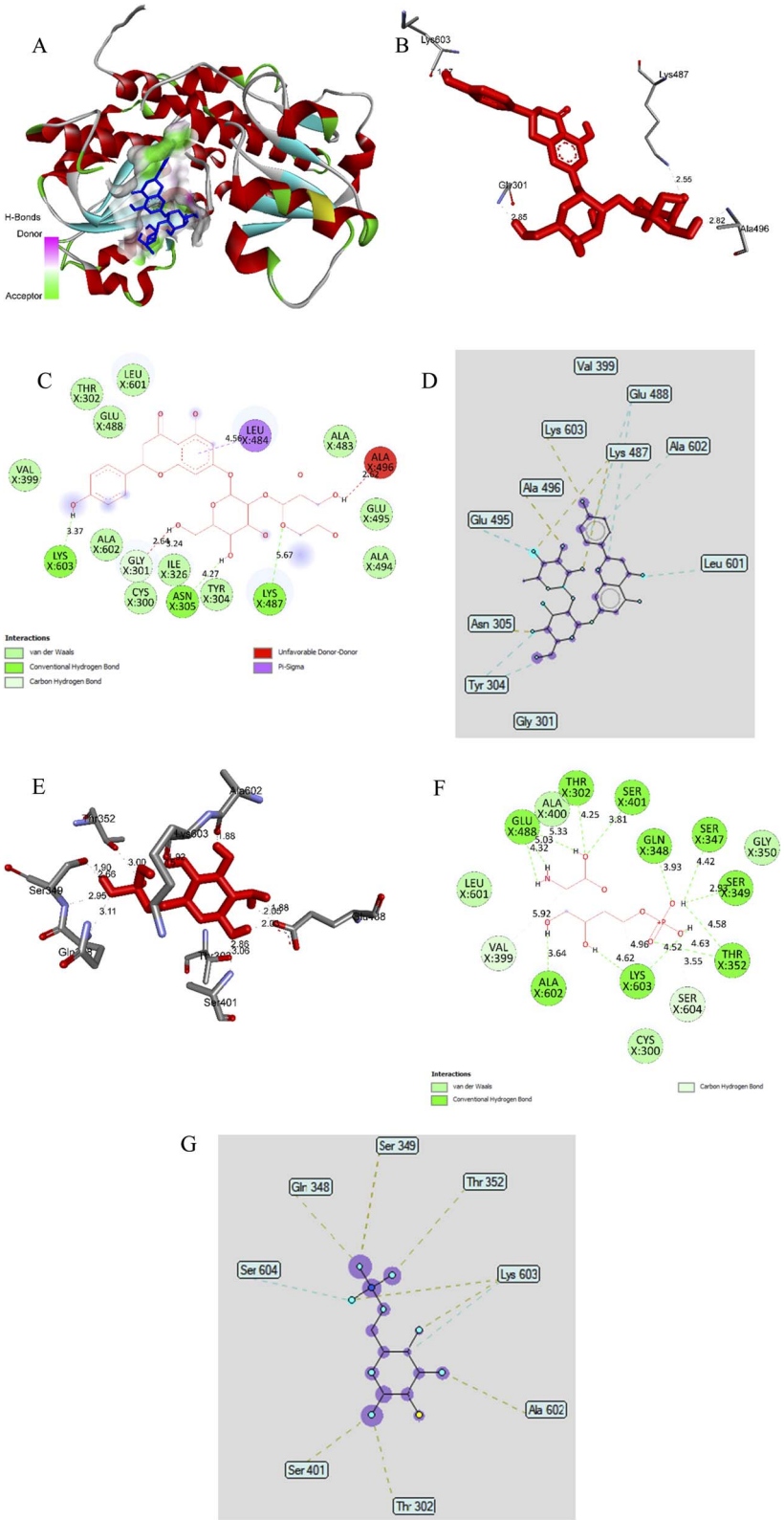

Fig. 9 (A) The best docking pose 60 of ligand naringin docked to an enzyme pocket at an active center of enzyme 2VF5 (PDB) synthesised glucosamine-6-phosphate present in cell wall of bacteria or fungi; (B) the hydrogen bonds linked from active atom on pose 60, ligand naringin to active residual amino acids on enzyme 2VF5; (C) a 2D diagram described the significant ligand interactions between pose 60 and enzyme 2VF5; (D) the ligand map exposed the secondary interactions between the best docking pose 60 and enzyme 2VF5; (E) the hydrogen bonds formed from active residual amino acids on enzyme 2VF5 to active atom on pose 83, the small ligand available in enzyme 2VF5; (F) a 2D diagram presented the important ligand interactions between pose 83 and enzyme 2VF5; (G) the ligand map exposed the secondary interactions between pose 83 and enzyme 2VF5.

interactions, they were hydrophobic interactions. As seen in Fig. 9G, a ligand map indicated secondary interactions that linked active atoms on pose 83 to active residual amino acids on the enzyme were weak interactions. Based on thermodynamic site and ligand interaction model, the interaction between ligand naringin and pose 60 was determined to be stronger than that of pose 83. Pose 60 was analysed as having a weak interaction with enzyme 2VF5 and this was also compatible with the *in vitro* test on the antifungal activity of naringin.

In this work, fluconazole (pose 87, the most stable conformation of the ligand fluconazole) was used as a reference drug and used in anti-fungi activity anchored to the target enzyme 2VF5, with the values of free Gibbs energy and inhibition constant of -5.55 kcal mol^{-1} and 86.10 μM, respectively, as shown in Fig. 10A and Table S9.† This pose formed four hydrogen bonds from residual of amino acids on enzymes such as Thr 302, Ser303, Ser 349, and Cys 300 to the active atom on pose 87. The significant ligand interactions between pose 87 and residual amino acids of enzyme indicated that Fluconazole interacted well with the enzyme because three parts of this pose, including the capping group (identification protein *via* aromatic or heterocyclic), connecting unit (linker, the aliphatic chains, and hydrophobic interactions) and functional groups (polar groups and hydrophilic interactions) were well identified *via* ligand interactions (Fig. 10B). The capping group detected by π-alkyl interactions from Ala 299 to triazole ring, π-sulphur from Cys 300 to triazole ring, π-donor hydrogen bonds from Thr 352, Ser 303 to triazole ring, another π-donor hydrogen from

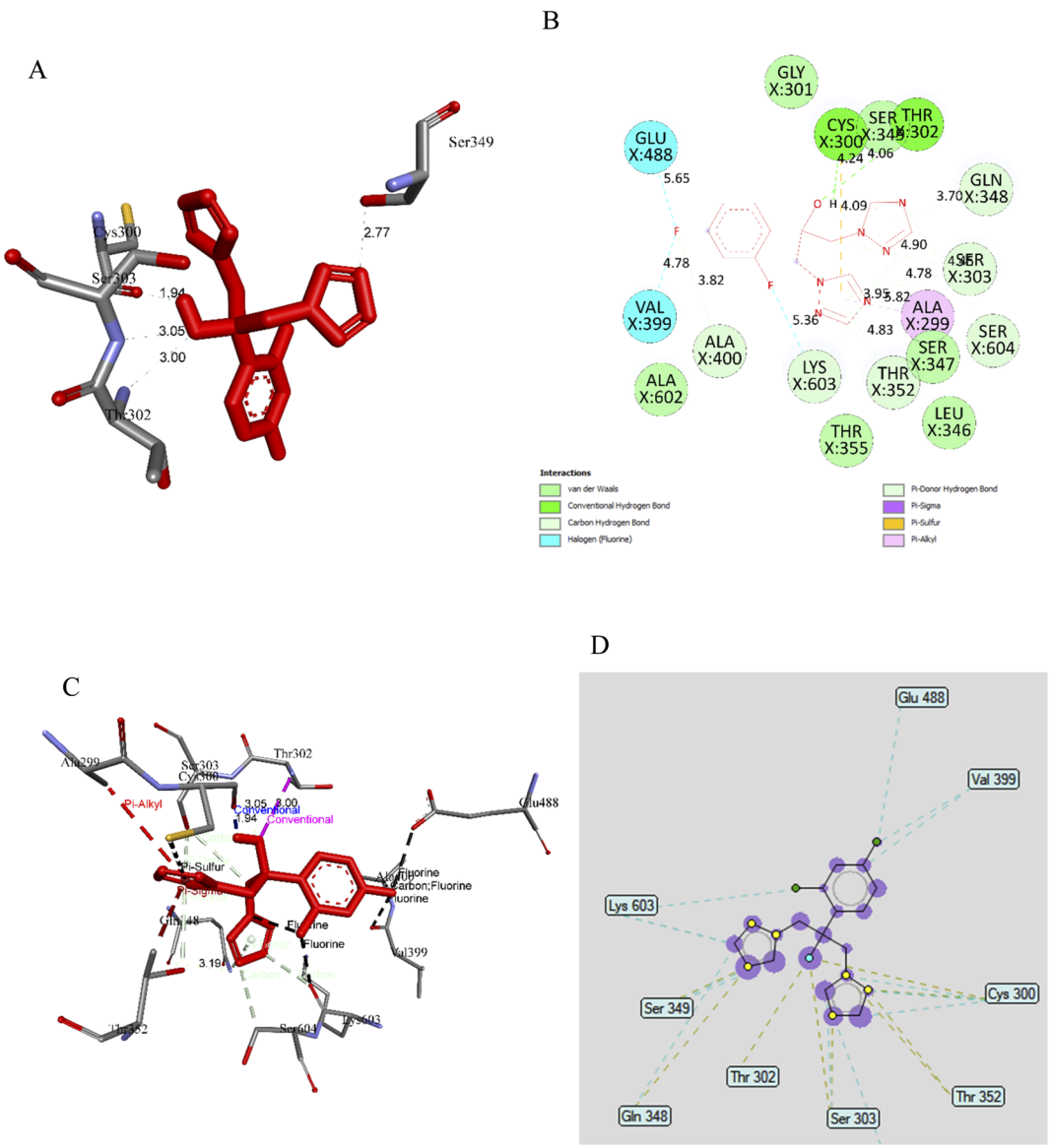

Fig. 10 (A) Pose 87, ligand fluconazole formed hydrogen bonding with active atoms on enzyme target, 2VF5; (B) a 2D diagram showed the significant ligand interactions between pose 87 and residual amino acids on enzyme 2VF5; (C) a 3D diagram showed the significant ligand interactions between pose 97 and residual amino acids on enzyme 2VF5; (D) ligand map indicated the secondary interactions between residual active amino acids of enzyme 2VF5 and active atoms on pose 87.

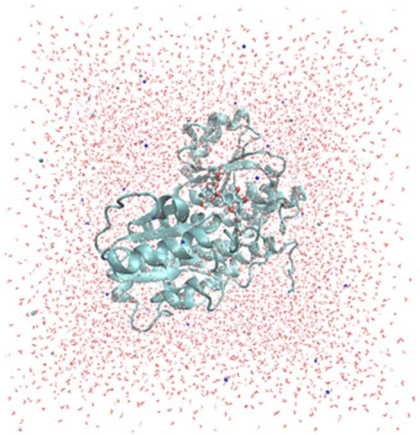

(A)

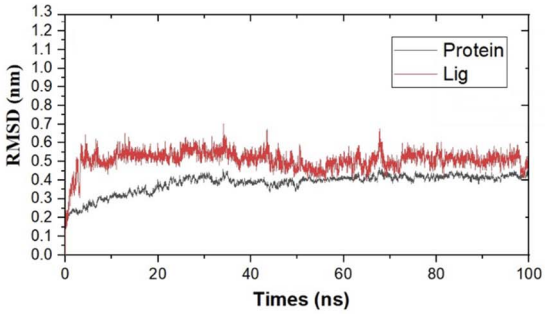

(B)

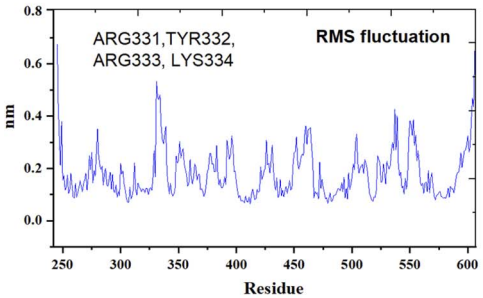

(C)

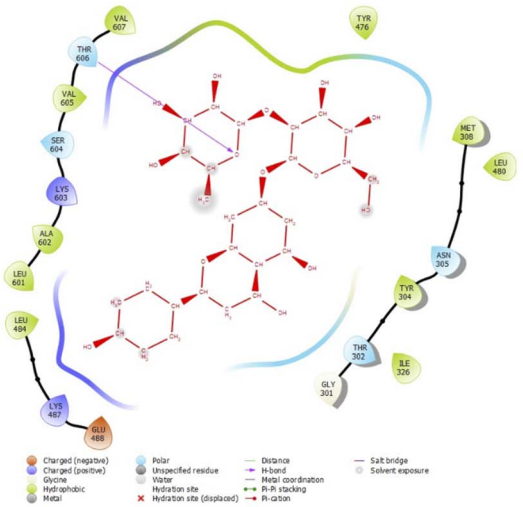

(D)

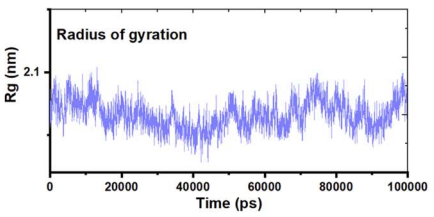

(E)

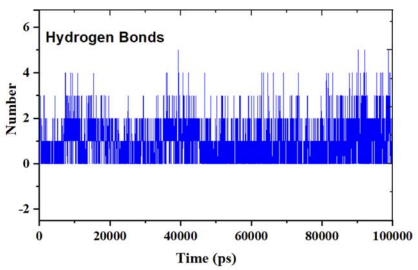

(F)

Fig. 11 (A) Protein–naringin complex (pose 60) in three-point transferable intermolecular potential water box. (B) The graph of RMSD studies for the protein (2VF5.pdb) in the presence of pose 60; (C) the root mean square fluctuation (RMSF); (D) the significant ligand interactions between pose 60 and enzyme 2VF5; (E) the complex-pose 60 radius of gyration (R_g); (F) the number of H bonds formed between pose 60 and crystal structure of enzyme 2VF5 was determined using 100 ns simulation trajectories.

Gln 348, Ser 604, Lys603 to another triazole ring. The connecting unit (CU) was identified by a π-donor hydrogen bond from Ser 303 to the methylene group of the pose, a hydrophobic interaction. The functional groups of pose 87 were detected by hydrogen bonds from Cys 300 to the hydrogen atom and Thr 302 to the oxygen atom of the alcohol group and halogen interactions, fluorine interactions from Glu 488, Val 399 to fluorine atoms on aromatic rings. Fig. 10C indicated that the essential ligand interactions between pose 87 and enzyme 2VF5 (3D diagram) were determined to be similar to 2D interactions in Fig. 10B. The ligand map exposed the secondary interactions such as hydrogen bonds (brown lines), from Gln 348, Thr 302, Ser 303, Thr 352, and Cys 300 to active atoms on pose 87, steric interactions, green coloured lines from Glu 488, Val 399, Cys 300, Thr 352, Ser 303, Gln 348, Ser 349, and Lys 603 to active atom on pose 87, overlap interactions, and violet circles, indicating that the bigger violet circles were the stronger overlap interactions of the poses (Fig. 10D). In this case, many amino acids were witnessed forming around this pose and proved that the ligand interactions between pose and enzyme were very strong in conformation processing of ligand fluconazole or pose 87. Based on thermodynamic site and ligand interactions, the enzyme inhibition ability was arranged as the following ranking: pose 87 (fluconazole) > pose 60 (naringin) > pose 83 (small ligand).

3.2.5. Molecular dynamics simulations analysis. MD was performed to examine the ligand's binding effectiveness toward the protein over time at atomic level. Several characteristics, including RMSD, RMSF, radius of gyration, and hydrogen bonds play major role in providing information of binding pattern. As a result, a 100 ns MD simulation study was done to compare with 3D-structure of glucosamine-6-phosphate synthase enzyme 2VF5 in order to evaluate the overall stability and binding effectiveness of pose 60, the best docking pose, ranked pose of ligand naringin as shown in Fig. 11A. RMSD parameter analysis provides detailed structure information for understanding the conformational stability of the system. Thus, RMSD studies for the protein (2VF5.pdb) in the presence of pose 60 were performed. After 50 ns of simulation, the analysis showed that the protein–pose 60 complex is highly equilibrated and stable (Fig. 11B). The close interaction of the ligand-complex shows that the protein–pose 60 complex is stable throughout the interaction process. The ligand fluctuated a little bit within its limit before 50 ns. The root mean square fluctuation (RMSF) method examines the flexibility of protein residues in the presence of pose 60, as shown in Fig. 11C, the protein–pose 60 complex exhibited a nearly identical fluctuation pattern, confirming the constrained motions over the 100 ns simulation. However, some residues namely ARG331, TYR332, ARG333, and LYS334 were not directly involved in the catalytic site that had some level of mobility with fluctuations ranging from 0.2 to 0.5 nm (Fig. 11D), indicating non-significant, whereas residues involving in the catalytic site to form the best pose with pose 60 had significant dynamic behavior that led to a stable protein–pose 60 complex. In addition, the complex-pose 60 radius of gyration (R_g) was measured as shown in Fig. 11E. The compactness of protein is indicated by the radius of gyration as a result of thermodynamic effects during the molecular dynamics simulation's 100 ns of protein folding and unfolding structures. For protein–ligand complexes, R_g values are shown in nanometer in Fig. 11E. Due to the dynamic behavior of the protein–pose 60 complex, the R_g values of the best docking pose under MD simulation were initiated at 2.05 nm, and the structure gradually increased and decreased under the limit (the complex having ions and solvent molecules during the MD simulation process). The system's R_g value is held constant throughout the entire procedure. The R_g value decreased from 2.1 to 2.0 nm at 40 ns before rising again to return the system to its original position, demonstrating that the receptor-pose 60 was stable and tightly packed. The number of H-bonds included in the MD simulation was counted using the gmx hbond. The number of H-bonds formed between pose 60 and protein, 2VF5: PDB was determined using 100 ns simulation trajectories, illustrated in Fig. 11F. The majority of hydrogen bonds in protein–pose 60 are between 2 and 3, followed by 4 and 5. As a result, this output aids the ligand in remaining stable with no changes in RMSD value during the simulation period. These results contributed to the stability of the protein–ligand complex by showing a continuous stable equilibrium during simulation.

4. Conclusion

The supercritical CO_2 technology was effectively used for the extraction of essential oils and naringin from waste pomelo peels. The composition of D-limonene in essential oil was significantly enhanced *via* this technique. Both natural products were evaluated *in vitro*—antimicrobial activity, giving the essential oil revealed its high activity against three bacterial strains, *M. catarrhalis*, *S. pyogenes*, and *S. pneumoniae*. Meanwhile, naringin indicated good inhibition towards all tested microbial strains. Particularly, naringin appeared to be a high inhibition compound against fungal strains, *T. rubrum*, *T. mentagrophytes*, and *M. gypseum*. For the computational study, the molecular docking model and the validation of the docking model confirmed that D-limonene inhibited well against the bacterium *M. catarrhalis*. The molecular docking model of naringin and its MD simulation showed that this compound possessed potential ligand interactions, which then confirmed it as an effective inhibiting factor against fungi.

Conflicts of interest

No potential conflict of interest was reported by the authors.

Acknowledgements

This work was funded by Ho Chi Minh City Department of Science and Technology (HCMC-DOST) under the grant number 37/2020/HĐ-QPTKHCN.

References

1 R. J. Anmol, S. Marium, F. T. Hiew, W. C. Han, L. K. Kwan, A. K. Y. Wong, F. Khan, M. M. R. Sarker, S. Y. Chan and

N. Kifli, *J. Evidence-Based Integr. Med.*, 2021, **26**, 2515690X211043741.
2 H. Hussain, N. Z. Mamadalieva, A. Hussain, U. Hassan, A. Rabnawaz, I. Ahmed and I. R. Green, *Curr. Issues Mol. Biol.*, 2022, **44**, 1960–1994.
3 Y. Zhao and S. Liu, *Pharmazie*, 2021, **76**, 359–363.
4 R. Chen, Q.-L. Qi, M.-T. Wang and Q.-Y. Li, *Pharm. Biol.*, 2016, **54**, 3203–3210.
5 S. Mahanta, B. Khanikor and R. Sarma, *J. Entomol. Zool. Stud.*, 2017, **5**, 803–809.
6 N.-G. Tao and Y.-J. Liu, *Int. J. Food Prop.*, 2012, **15**, 709–716.
7 K. Sudto, S. Pornpakakul and S. Wanichwecharungruang, *Int. J. Food Sci. Technol.*, 2009, **44**, 1737–1742.
8 P. A. Uwineza and A. Waśkiewicz, *Molecules*, 2020, **25**, 3847.
9 T. T.-T. Huynh, T.-C. Mai, C.-H. Dang, T. T.-T. Vo, D.-T. Nguyen, V.-S. Dang, K. D. V. Nguyen, V.-T. Tran and T.-D. Nguyen, *Arabian J. Chem.*, 2020, **13**, 7289–7301.
10 I. Quispe-Fuentes, E. Uribe, J. López, D. Contreras and J. Poblete, *J. Food Process. Preserv.*, 2022, **46**, e16116.
11 B. Su, J. Tian, M. Liu, K. Wang, W. Yang, J. Ning, Y. Li and G. Zheng, *J. Sep. Sci.*, 2022, **45**(15), 3031–3042.
12 A. N. Giannuzzo, H. J. Boggetti, M. A. Nazareno and H. T. Mishima, *Phytochem. Anal.*, 2003, **14**, 221–223.
13 J. Yu, D. V. Dandekar, R. T. Toledo, R. K. Singh and B. S. Patil, *Food Chem.*, 2007, **105**, 1026–1031.
14 M. Hoshino, T. Suetsugu, H. Iwai, A. Takamizu, M. Tanaka, A. Quitain, M. Sasaki and M. Goto, *Trans. Mater. Res. Soc. Jpn.*, 2014, **39**, 309–311.
15 S. Rajput, S. Kaur, P. S. Panesar and A. Thakur, *Biomass Convers. Biorefin.*, 2022, 1–10.
16 R. Romano, L. De Luca, A. Aiello, D. Rossi, F. Pizzolongo and P. Masi, *Int. J. Food Sci. Technol.*, 2022, **57**, 3826–3837.
17 D. W. Ingersoll, P. M. Bronstein and J. Bonventre, *J. Comp. Physiol. Psychol.*, 1976, **90**, 198.
18 T. T. A. My, H. T. P. Loan, N. T. T. Hai, L. T. Hieu, T. T. Hoa, B. T. P. Thuy, D. T. Quang, N. T. Triet, T. T. V. Anh and N. T. X. Dieu, *ChemistrySelect*, 2020, **5**, 6312–6320.
19 B. T. P. Thuy, T. T. A. My, N. T. T. Hai, L. T. Hieu, T. T. Hoa, H. Thi Phuong Loan, N. T. Triet, T. T. V. Anh, P. T. Quy and P. V. Tat, *ACS Omega*, 2020, **5**, 8312–8320.
20 B. L. Staker, M. D. Feese, M. Cushman, Y. Pommier, D. Zembower, L. Stewart and A. B. Burgin, *J. Med. Chem.*, 2005, **48**, 2336–2345.
21 T.-B.-N. Dao, T.-M.-T. Nguyen, V.-Q. Nguyen, T.-M.-D. Tran, N.-M.-A. Tran, C. H. Nguyen, T.-H.-T. Nguyen, H.-H. Nguyen, J. Sichaem and C.-L. Tran, *Molecules*, 2021, **26**, 2531.
22 M. Aliye, A. Dekebo, H. Tesso, T. Abdo, R. Eswaramoorthy and Y. Melaku, *Sci. Rep.*, 2021, **11**, 1–12.
23 S. Singh, A. Datta, A. Schmidtchen, A. Bhunia and M. Malmsten, *Sci. Rep.*, 2017, **7**, 1–14.
24 K. Hałdys, W. Goldeman, M. Jewgiński, E. Wolińska, N. Anger, J. Rossowska and R. Latajka, *Bioorg. Chem.*, 2018, **81**, 577–586.
25 G. Brancolini, D. B. Kokh, L. Calzolai, R. C. Wade and S. Corni, *ACS Nano*, 2012, **6**, 9863–9878.
26 M. N. Sibanyoni, S. K. Chaudhary, W. Chen, H.-R. Adhami, S. Combrinck, V. Maharaj, D. Schuster and A. Viljoen, *Fitoterapia*, 2020, **146**, 104650.
27 E. W. Bell and Y. Zhang, *J. Cheminf.*, 2019, **11**, 1–9.
28 T.-H. Duong, A. P. Devi, N.-V. Huynh, J. Sichaem, H.-D. Tran, M. Alam, T.-P. Nguyen, H.-H. Nguyen, W. Chavasiri and T.-C. Nguyen, *Bioorg. Med. Chem. Lett.*, 2020, **30**, 127359.
29 G. L. Warren, C. W. Andrews, A.-M. Capelli, B. Clarke, J. LaLonde, M. H. Lambert, M. Lindvall, N. Nevins, S. F. Semus and S. Senger, *J. Med. Chem.*, 2006, **49**, 5912–5931.
30 P. Agrawal, H. Singh, H. K. Srivastava, S. Singh, G. Kishore and G. P. Raghava, *BMC Bioinf.*, 2019, **19**, 105–124.
31 F. Maltese, C. Erkelens, F. van der Kooy, Y. H. Choi and R. Verpoorte, *Food Chem.*, 2009, **116**, 575–579.
32 T. N.-T. Nguyen, T. N.-N. Huynh, V.-T. Tran, C.-H. Dang, T. K.-D. Hoang and T.-D. Nguyen, *J. Essent. Oil Res.*, 2018, **30**, 285–292.
33 M. Tuncbilek, T. Kiper and N. Altanlar, *Eur. J. Med. Chem.*, 2009, **44**, 1024–1033.
34 G. Giannini, W. Cabri, C. Fattorusso and M. Rodriquez, *Future Med. Chem.*, 2012, **4**, 1439–1460.
35 F. U. Eze, U. C. Okoro, D. I. Ugwu and S. N. Okafor, *Front. Chem.*, 2019, 634.
36 H. Berendsen, J. Grigera and T. Straatsma, *J. Phys. Chem.*, 1987, **91**, 6269–6271.
37 A. B. Hsouna, M. Trigui, R. B. Mansour, R. M. Jarraya, M. Damak and S. Jaoua, *Int. J. Food Microbiol.*, 2011, **148**, 66–72.
38 Y. Han, Z. Sun and W. Chen, *Molecules*, 2019, **25**, 33.
39 L. Yu, J. Yan and Z. Sun, *Mol. Med. Rep.*, 2017, **15**, 2339–2346.
40 J. A. Miller, P. A. Thompson, I. A. Hakim, H.-H. S. Chow and C. A. Thomson, *Oncol. Rev.*, 2011, **5**, 31–42.
41 V. M. Grinevicius, K. S. Andrade, F. Ourique, G. A. Micke, S. R. Ferreira and R. C. Pedrosa, *J. Supercrit. Fluids*, 2017, **128**, 94–101.
42 R. P. Adams, *Identification of essential oil components by gas chromatography/mass spectrometry*, Allured publishing corporation, Carol Stream, 2007.
43 V.-D. Doan, V.-T. Le, T.-L. Phan, T. L.-H. Nguyen and T.-D. Nguyen, *J. Cluster Sci.*, 2021, **32**, 1673–1682.
44 M.-T. Tran, L.-P. Nguyen, D.-T. Nguyen, L. Cam-Huong, C.-H. Dang, T. T. K. Chi and T.-D. Nguyen, *Res. Chem. Intermed.*, 2021, **47**, 4613–4633.
45 G. A. Subramenium, K. Vijayakumar and S. K. Pandian, *J. Med. Microbiol.*, 2015, **64**, 879–890.
46 M. T. I. Salama, *J. Essent. Oil-Bear. Plants*, 2017, **20**, 233–239.
47 F. Wang, H. You, Y. Guo, Y. Wei, P. Xia, Z. Yang, M. Ren, H. Guo, R. Han and D. Yang, *Ind. Crops Prod.*, 2020, **147**, 112172.
48 A. Tan, L. V. Blakeway, Y. Yang, Y. Zhou, J. M. Atack, I. R. Peak and K. L. Seib, *PLoS One*, 2020, **15**, e0234306.
49 S. Andrade-Ochoa, K. F. Chacón-Vargas, L. E. Sánchez-Torres, B. E. Rivera-Chavira, B. Nogueda-Torres and G. V. Nevárez-Moorillón, *Membranes*, 2021, **11**, 405.